The University of Sydney

School of Civil Engineering
Sydney NSW 2006
AUSTRALIA

http://www.civil.usyd.edu.au/

Centre for Advanced Structural Engineering

Bifurcation of Locally Buckled Point Symmetric Columns – Experimental Investigations

Research Report No R867

Kim JR Rasmussen, MScEng, PhD

March 2006

ISSN 1833-2781

The University of Sydney

School of Civil Engineering
Centre for Advanced Structural Engineering
http://www.civil.usyd.edu.au/

Bifurcation of Locally Buckled Point Symmetric Columns – Experimental Investigations

Research Report No R867

Kim Rasmussen, MScEng, PhD

March 2006

Abstract:

The bifurcation equations for locally buckled point symmetric sections are derived in a companion report [1]. In the present report, two series of experiments are reported, one on narrow flange Z-sections and one on wide flange Z-sections. The main objective of the tests was to validate the bifurcation load predictions derived in [1] against experimental values. A further objective of the tests on narrow flange sections was to investigate the change in the direction of overall buckling, as predicted by the theory, from principal axis directions to non-principal directions. A further objective of the tests on wide flange sections was to investigate the possible change of the critical overall buckling mode from a flexural mode to a torsional mode as a result of local buckling. Agreement is generally found between analytical and experimental results.

Keywords:

Z-sections, steel structures, tests, local buckling, torsional buckling, flexural buckling, interaction buckling, bifurcation analysis, finite strip analysis, finite element analysis.

Copyright Notice

School of Civil Engineering, Research Report R867
Bifurcation of Locally Buckled Point Symmetric Columns – Experimental Investigations

K.Rasmussen@civil.usyd.edu.au

Published by:
School of Civil Engineering
The University of Sydney
Sydney NSW 2006
AUSTRALIA

March 2006

This report and other Research Reports published by The School of Civil Engineering are available on the Internet:

http://www.civil.usyd.edu.au

Table of Contents

1 Introduction

It is well-known that local buckling may influence the overall buckling behaviour of thin-walled sections. The influence depends on the end support conditions (*e.g.* simply supported or fixed) and the symmetry characteristics. For a doubly symmetric section, such as an I-section, local buckling reduces the flexural rigidity and precipitates overall buckling at a reduced load but does not induce overall displacements. For a singly symmetric cross-section, such as a channel section, local buckling induces overall bending when the column is compressed between pinned ends but not when compressed between fixed ends [2].

The present report focuses on the bifurcation of locally buckled point symmetric columns, such as Z-section columns, as shown in Fig. 1. Theoretical results [1] have shown that local buckling of point symmetric columns does not induce overall displacements, as it does in pin-ended singly symmetric columns, but causes a coupling between the minor and major axis buckling displacements. In physical terms, this implies that the direction of overall buckling occurs about an axis rotated from the minor principal axis.

According to the theory [1], torsional and flexural overall buckling of point symmetric sections are uncoupled. However, the torsional buckling mode may become critical in the case of Z-sections with very slender flanges because local buckling reduces the warping rigidity (EI_ω) more severely than the minor axis flexural rigidity (EI_y). The purpose of this report is to present tests and finite element analyses of fixed-ended Z-section columns to verify experimentally and numerically the behaviour predicted by the theory.

Two test series are reported, one on narrow flange Z-sections and one on wide flange Z-sections. The tests specimens were manufactured from high strength steel by brake-pressing, and so contained low levels of residual stress. Fixed-ended column tests were performed at eight and nine different lengths for the narrow and wide flange test series respectively, covering the range from stub columns to long columns.

2 Buckling Equations

It is shown in a companion report [1] that the longitudinal buckling displacement w_b, the flexural buckling displacements u_b and v_b in the principal x- and y-axis directions respectively, and the buckling twist rotation ϕ_b are determined from the differential equations,

$$\left((EA)_t \dot{w}_b'\right)' - \left((ES_\omega)_t \dot{\phi}_b''\right)' = 0 \tag{1}$$

$$-\left((ES_\omega)_t \dot{w}_b'\right)'' + \left((EI_\omega)_t \dot{\phi}_b''\right)'' - \left((GJ)_t \phi_b'\right)' + \left(N_{cr} \frac{\overline{W}}{\overline{N}} \phi_b'\right)' = 0 \tag{2}$$

$$\left((EI_y)_t \dot{u}_b''\right)'' + \left((EI_{xy})_t \dot{v}_b''\right)'' + \left(N_{cr} u_b'\right)' = 0 \tag{3}$$

$$\left((EI_{xy})_t \dot{u}_b''\right)'' + \left((EI_x)_t \dot{v}_b''\right)'' + \left(N_{cr} v_b'\right) = 0 \tag{4}$$

where N_{cr} is the overall buckling load, $(EA)_t$, $(ES_\omega)_t$, $(EI_x)_t$, $(EI_y)_t$, $(EI_{xy})_t$, $(EI_\omega)_t$, $(GJ)_t$ are tangent rigidities calculated at the buckling load, and

$$\frac{\overline{W}}{\overline{N}} = \frac{\int_A \sigma_0 \left(x^2 + y^2\right) dA}{\int_A \sigma_0 dA} \tag{5}$$

In eqn. 5, σ_0 is the longitudinal stress at incipient overall buckling. The tangent rigidities ($(EA)_t$, $(ES_\omega)_t$, $(EI_x)_t$, $(EI_y)_t$, $(EI_{xy})_t$, $(EI_\omega)_t$) can be found by subjecting a length of section equal to the local buckle half-wavelength to increasing levels of compression and then superimposing small increments of generalized strain (axial compression, curvature about the major and minor principal axes, and warping) at each compression level. The tangent rigidities are the ratios of the resulting stress resultant to the applied generalised strain, see Refs [1-3] for details. A nonlinear inelastic finite strip local buckling analysis [4] has been used in this report to calculate the tangent rigidities.

For fixed-ended columns, the governing equations (1-4) and the boundary conditions are satisfied by the displacement field,

$$\frac{w_b}{C_w} = \sin\left(\frac{2\pi z}{L}\right) \tag{6}$$

$$\frac{u_b}{C_u} = \frac{v_b}{C_v} = \frac{\theta_b}{C_\theta} = 1 - \cos\left(\frac{2\pi z}{L}\right) \tag{7}$$

which, upon substitution into eqns (1-4), leads to an eigenvalue problem with the following non-trivial solutions [1],

$$N_{cr\,\varphi} = \frac{\overline{N}}{\overline{W}} \left(\frac{4\pi^2 \left(EI_\omega\right)_t}{L^2} + \left(GJ\right)_t - \frac{4\pi^2}{L^2} \frac{\left(ES_\omega\right)_t^2}{\left(EA\right)_t} \right) \tag{8}$$

$$N_{cr\,uv} = \frac{-B \pm \sqrt{B^2 - 4AC}}{2A} \tag{9}$$

where

$$A = 1 \tag{10}$$

$$B = -(N_x + N_y) \tag{11}$$

$$C = N_x N_y - \left(\frac{2\pi}{L}\right)^4 \left(EI_{xy}\right)_t^2 \tag{12}$$

$$N_x = \frac{4\pi^2 \left(EI_x\right)_t}{L^2} \tag{13}$$

$$N_y = \frac{4\pi^2 \left(EI_y\right)_t}{L^2}. \tag{14}$$

3 Experimental Investigations

3.1 Narrow Flange Z-sections

3.1.1 Material Properties

The test specimens were brake-pressed into section from nominally 1.5 mm thick G500 sheet steel. G500 is an Australian produced steel to AS1397 [5] with galvanized coating and nominal yield stress of 500 MPa. It has a low tensile strength to yield stress ratio and limited ductility of the order of 10-15%.

Five tensile coupons were cut from steel sheets in the same direction as the longitudinal axis of the test specimens. Figures 2a and 2b show a typical stress-strain curve obtained from one of the coupon tests. The average values of initial Young's modulus (E_0), yield stress (σ_y) and ultimate tensile strength (σ_u) are shown in Table 1. The COV of E_0, σ_y and σ_u based on the five tests were 0.039, 0.0039 and 0.003 respectively indicating close resemblance of the mechanical properties. The sheets probably pertained to the same batch.

In the absence of a sharp yield point, the yield stress was obtained as the 0.2% proof stress. Significant softening was observed in the vicinity of yield, as shown in Fig. 2a. Based on an average value of 0.01% proof stress of $\sigma_{0.01}$=383 MPa, as determined from the stress-strain curves, the Ramberg-Osgood n-parameter was calculated as calculated as $n = \ln(20)/\ln(\sigma_{0.2}/\sigma_{0.01}) = 9.1$, as shown in Table 1.

3.1.2 Column tests

The average measured cross-section dimensions are shown in Table 2 using the nomenclature defined in Fig. 3a. The coefficients of variation of the measured widths of the flanges (b_f) and web (b_w) were 0.022 and 0.007 respectively, indicating that a tight tolerance was achieved on the cross-section dimensions. The average measured thickness (T) was 1.58 mm. After removing the galvanizing layer by etching, the base metal thickness (t) was measured as 1.495 mm. The b/t-ratios for the flanges and web were 17.1 and 80.5 respectively. The elastic local buckling stress (σ_l) and half-wavelength (l) were determined from a finite strip analysis [6], as also shown in Table 1. The local buckling mode is shown in Fig. 3b. Local buckling was precipitated by instability of the web.

The test specimens were cut in lengths varying from 250 mm to 1600 mm. Subsequently, the ends were milled flat to ensure even loading. For each length, two nominally identical specimens were prepared. Local and overall geometric imperfections were measured on all specimens prior to testing. The overall geometric imperfections are shown as u_0 in Table 3 corresponding to the measured out-of straightness at mid-length in the direction of the major x-axis, as shown in Fig. 3c. The out-of-flatness of the web (w_{w0}) measured at the centre of the web at mid-length is also shown in Table 3. The averages of the overall imperfection relative to the length (u_0/L) and the local imperfection of the web (w_{w0}) were 1/4050 and 0.19 mm respectively.

The specimens were loaded between fixed ends in a vertical position. The top end platen was rigidly connected to the cross-head, thus preventing flexural and torsional rotations. At the base, a lockable spherical seat was used to ensure full contact between the end platen and the specimen during setup. Once contact was achieved, the seat was locked by tightening a bolt

at each corner such that flexural and torsional rotations could no longer occur. The platens also restrained torsional warping displacements.

The specimens were uniformly compressed until failure using a 300 kN capacity MTS Sintech testing machine. The ultimate load (N_u) was recorded, as shown in Table 3, and the test then continued into the post-ultimate range. Readings of local and overall deformations were taken at regular intervals. Local deformations were measured using transducers mounted on an aluminium frame, which was attached to the corners of the specimen at mid-length, as shown in Fig. 4. The frame followed the specimen during overall buckling and ensured that the local buckling deformations were measured at the same points in the cross-section throughout loading. Readings were taken at the centre of the web and near the free edge of the flanges. Two transducers were used at each of these locations, spaced approximately a quarter-wave longitudinally to ensure non-zero local buckling readings from at least one of the two sets of transducers. In addition, three transducers were used to record overall displacements at mid-length. Local buckling of the web and flanges can be clearly seen in Fig. 4.

The experimental local buckling load was estimated using the N *vs* w^2 method, according to which the local buckling load is the intersection of the load axis with the line fitted through the graph of the load (N) versus the square of the plate buckling deformation in the initial post buckling range. The experimental local buckling loads (N_{lE}) are shown in Table 3. They are generally close with an average of 35.3 kN and a COV of 0.053. The average experimental local buckling load (N_{lE}=35.3 kN) was nearly equal to the theoretical value (N_l=35.2 kN).

3.1.3 Comparison of experimental and numerical results

Figure 5 compares buckling curves determined from Eqns (8-14) with the test strengths shown in Table 3. The buckling curves are those corresponding to elastic material behaviour and elastic perfectly-plastic material behaviour with values of Young's modulus (E_0) and yield stress (σ_y) as shown in Table 1. The Euler curve assuming no local buckling is also included. The base metal thickness and average measured values of flange and web widths were used in the numerical calculations, as shown in Table 2. A local geometric imperfection was incorporated in the nonlinear finite strip analysis, assumed to be in the shape of the critical local buckling mode with a magnitude at the centre of the web of w_{w0}=0.19 mm. This value was the average measured local geometric imperfection, as shown in Table 3, and was chosen according to the recommendation made in [7]. Corner radii were ignored in the numerical analyses. One and two harmonics were used to model out-of-plane (flexural) and in-plane (membrane) buckling displacements respectively. The overall buckling loads and test strengths are nondimensionalised with respect to the local buckling load (N_l=35.2 kN) in Fig. 5.

It follows from Fig. 5 that the elastic and inelastic bifurcation curves are somewhat higher than the test strength. At intermediate and long lengths, the discrepancy may be explained by the presence of overall geometric imperfections in the test specimens of average magnitude of L/4050, which were not negligible. At short lengths, it is noted that the plateau reached by the inelastic bifurcation curve at a length of about 750 mm is a measure of the stub column strength predicted by the finite strip analysis, and that the plateau is 15 % higher than the experimental stub column strength obtained from the tests on 250 mm long columns. The latter result suggests that the displacement field used in the finite strip analysis may not have been adequate for analysing the localised deformations developing near the ultimate load, as

observed in the tests. Furthermore, the material suffered gradual softening, which would reduce the bifurcation loads, and was not elastic perfectly-plastic as assumed in the finite strip analysis.

The twist rotation was calculated from the three overall transducers located at mid-length. It was found to be negligible at the ultimate load for all specimens, thus confirming that local buckling does not produce coupling between torsion and flexure in the bifurcation of point-symmetric sections.

3.1.4 Direction of overall buckling

According to the classical theory for non-locally buckled point-symmetric sections, overall flexural buckling occurs about the minor *y*-axis and is uncoupled from flexural buckling about the major *x*-axis. However, it follows from eqns (3,4) that for a locally bucked section, flexural buckling about the minor principal axis is coupled with flexural buckling about the major principal axis. From a physical viewpoint, this means that the direction of overall buckling deviates from that of the major *x*-axis. Elastically, the change occurs because the section loses stiffness near the tips of the flanges which causes the axis of buckling to align itself more with the axis through the web.

By substituting eqn. (7) into eqns (3,4), the following eigenvalue equation results,

$$\begin{bmatrix} \left(\frac{2\pi}{L}\right)^2 (EI_y)_t - N_{cr} & \left(\frac{2\pi}{L}\right)^2 (EI_{xy})_t \\ \left(\frac{2\pi}{L}\right)^2 (EI_{xy})_t & \left(\frac{2\pi}{L}\right)^2 (EI_x)_t - N_{cr} \end{bmatrix} \begin{bmatrix} C_u \\ C_v \end{bmatrix} = \begin{bmatrix} 0 \\ 0 \end{bmatrix} \tag{15}$$

from which the change in rotation ($\Delta\alpha$) of the axis of buckling can be determined,

$$\Delta\alpha = \tan^{-1}\left(\frac{v_b}{u_b}\right) = \tan^{-1}\left(\frac{C_v}{C_u}\right) = \tan^{-1}\left(\frac{\left(\frac{2\pi}{L}\right)^2 (EI_{xy})_t}{\left(\frac{2\pi}{L}\right)^2 (EI_x)_t - N_{cr}} \right). \tag{16}$$

Equation (16) is plotted against the nondimensionalised load (N/N_l) in Fig. 6 for both the elastic and inelastic cases. In the inelastic case, the axis of buckling first rotates towards the web, then starts rotating back toward the principal y-axis direction at a load of about N/N_l=1.9. The latter change in axis of rotation is a result of the fact that when membrane yield occurs near the corners, the material loses stiffness in this region causing the axis of rotation to rotate away from the axis through the web.

It was sought to verify the predicted change in direction of overall buckling using the experimental plots of major (u) and minor (v) axis overall buckling displacements. However, as shown by the inelastic curve in Fig. 6, the change of angle ($\Delta\alpha$) was less than about 1° which could not be detected experimentally because overall geometric imperfections produced displacements in both principal directions from the onset of loading. While overall buckling principally occurred in the major *x*-axis direction, there was significant random variation in the calculation of $\Delta\alpha=\tan^{-1}(v/u)$.

A geometric nonlinear finite element analysis [8] was therefore performed on three lengths of column, L=800 mm, L=1000 mm and L=1200 mm, using SR4 shell elements for the discretisation of web and flanges. A local geometric imperfection was introduced with the same magnitude (w_{w0}=0.19mm) as that used in the nonlinear finite strip analysis. A small overall flexural geometric imperfection (u_0) of L/10,000 was also introduced to avoid numerical instability and/or possible skipping of the overall bifurcation point. The overall geometric imperfection was purely in the direction of the major x-axis. As for the nonlinear finite strip analysis, the width and thickness of the web and flanges, as well as the Young's modulus, were the average measured values given in Tables 1 and 2. The material was assumed to be linear-elastic.

The change in direction of overall buckling from the major principal direction ($\Delta\alpha=\tan^{-1}(v/u)$) was calculated using the values of u and v recorded at the ultimate load, as obtained from the nonlinear analysis. The points are labeled "Abaqus" in Figure 6 and seen to agree with the curve predicted by the bifurcation theory, particularly for ultimate loads less than twice the local buckling load.

3.2 Wide flange section

3.2.1 Material properties

The test specimens were brake-pressed into section from nominally 1.5 mm thick G450 sheet steel. Two tensile and two compression coupons were cut from the steel sheets in the same direction as the longitudinal axis of the test specimens. The average values of initial Young's modulus (E_0), yield stress (σ_y) and ultimate tensile strength (σ_u) are shown in Table 4. As for the G500 material used for the tests on narrow flange sections, significant softening was observed in the vicinity of yield, and hence the yield stress (σ_y) was obtained as the 0.2% proof stress. The Ramberg-Osgood n-parameters shown in Table 4 are based on the average values of 0.01% proof stress ($\sigma_{0.01}$) and 0.2% proof stress ($\sigma_{0.2}$), as determined from the stress-strain curves.

3.2.2 Column tests

The average measured cross-section dimensions are shown in Table 5. The coefficients of variation of the measured widths of the flanges (b_f) and web (b_w) were 0.013 and 0.023 respectively, indicating that a tight tolerance was achieved on the cross-section dimensions. The average base metal thickness (t) was 1.50 mm, measured after removing the galvanizing layer by etching. The b/t-ratios for the flanges and web were 26.7 and 26.3 respectively. The elastic local buckling stress (σ_l) and half-wavelength (l) are also shown in Table 5, as determined from a finite strip analysis [6]. The local buckling mode, critical overall flexural buckling mode and overall torsional mode are shown in Figs 7b, 7c and 7d respectively.

The test specimens were cut in lengths varying from 120 mm to 1600 mm. Subsequently, the ends were milled flat to ensure even loading. For each length, two nominally identical specimens were prepared. Local and overall geometric imperfections were measured on all specimens prior to testing. The overall geometric imperfections are shown as u_0 and ϕ_0 in Table 6 corresponding to the measured out-of straightness at mid-length in the direction of the major x-axis, as shown in Fig. 7c, and the initial twist rotation at mid-length, as shown in

Fig. 7d. The out-of-flatness of the tip of the flanges (w_{f0}) measured at mid-length is also shown in Table 6. The values of w_{f0} were obtained as a mean of the values measured at each flange tip by adding or subtracting the values depending on whether their directions were sympathetic to the local buckling mode or not. The averages of the overall imperfection relative to the length (u_0/L) and the local imperfection of the flanges (w_{f0}) were 1/14400 and 0.20 mm respectively.

The specimens were loaded between fixed ends in the vertical position using the same procedure as that used for the narrow flange test specimens. Depending on the length, the specimens failed by torsional and/or flexural overall buckling. Figure 8 shows an example of combined torsional and flexural buckling of a locally buckled Z-section. The ultimate loads (N_u) are shown in Table 6. As for the narrow flange tests, the experimental local buckling load was estimated using the N *vs* w^2 method. The experimental local buckling loads (N_{lE}) are included in Table 6. They are generally close with an average of 41.1 kN and a COV of 0.039. The average experimental local buckling load (N_{lE}=41.1 kN) was close to the theoretical value (N_l=40.2 kN).

3.2.3 Comparison of experimental and numerical results

Figures 9a and 9b compare the test strengths shown in Table 6 with buckling curves determined from Eqns (8-14) for the magnitudes of local geometric imperfection of 0.02 mm and 0.2 mm respectively. The overall buckling loads and test strengths are nondimensionalised with respect to the theoretical local buckling load (N_l=40.2 kN). In the nonlinear post-local buckling analyses, the local geometric imperfection was assumed to be in the shape of the elastic local buckling mode. The buckling curves are those corresponding to elastic material behaviour and elastic perfectly-plastic material behaviour with values of Young's modulus (E_0) and yield stress (σ_y) determined from the compression coupon tests, as shown in Table 4. The base metal thickness and average measured values of flange and web widths were used in the numerical calculations, as shown in Table 5, ignoring corner radii. One and two harmonics were used to model out-of-plane (flexural) and in-plane (membrane) buckling displacements respectively.

Figures 9a and 9b show the elastic and inelastic bifurcation curves of the locally buckled (distorted) cross-section, as well as the classical elastic overall flexural and torsional buckling curves assuming no local buckling. According to classical theory, the critical overall mode is the flexural mode at all lengths. However, for small local geometric imperfections, the critical overall mode switches to a torsional mode in the short and intermediate length range, as demonstrated by the elastic and inelastic buckling curves shown in Fig. 9a. Torsional buckling becomes less critical for larger values of local geometric imperfection, as shown in Fig. 9b.

The experimental failure modes (local, torsional and/or flexural) are also shown in Figs 9a and 9b. The overall failure modes were determined by comparing the curvature about the minor axis (κ_u) with the rate of change of twist (κ_ϕ) at the ultimate load. Using the buckling functions given by eqn. 7, the minor axis curvature and rate of change of twist were obtained as,

$$\kappa_u = -\left(\frac{2\pi}{L}\right)^2 u_{b_M} \cos\left(\frac{2\pi z}{L}\right) \tag{17}$$

$$\kappa_\phi = \left(\frac{2\pi}{L}\right) \phi_{b_M} \sin\left(\frac{2\pi z}{L}\right) \tag{18}$$

where u_{bM} and ϕ_{bM} are the values of minor axis displacement and twist rotation at mid-span measured at the ultimate load respectively. The overall buckling mode was determined using the following criterion:

$$\text{Overall failure mode} = \begin{cases} \text{Torsional (T)} & \text{when } \left|\kappa_\phi(L/4)\right| > 2\left|\kappa_u(L/2)\right| \\ \text{Flexural and Torsional (F, T)} & \text{when } \tfrac{1}{2}\left|\kappa_u(L/4)\right| \le \left|\kappa_\phi(L/4)\right| \le 2\left|\kappa_u(L/2)\right| \\ \text{Flexural (F)} & \text{when } \left|\kappa_\phi(L/4)\right| < \tfrac{1}{2}\left|\kappa_u(L/2)\right| \end{cases} \tag{19}$$

The test strengths are shown with open or solid markers for overall minor axis geometric imperfections relative to the length (u_0/L) less than or greater than 1/10,000 respectively. The open markers thus represent the strength of nearly straight columns.

The bifurcation curves shown in Fig. 9a for w_{f0}=0.02 mm are generally in close agreement with the test strengths, particularly those with overall geometric imperfections less than L/10,000. The slight discrepancy is attributed mainly to the facts that a) the bifurcation analysis assumes perfect column geometry and so does not consider overall geometric imperfections (albeit small), b) the loss of stiffness at low stress values implied by the nonlinearity of the stress-strain curve was not considered in the nonlinear analysis used to calculate the inelastic tangent stiffness values, and c) the overall bifurcation loads are sensitive to local geometric imperfections. Overall geometric imperfections mainly affect the column strength in the intermediate to long length range, while the nonlinear stress-strain curve most significantly affects the column strength in the short to intermediate length range where the buckling stress exceeds the proportionality stress.

The predicted and observed overall failure modes generally agree except that in several tests, torsional buckling occurred in combination with flexural buckling and in the tests of the 1400 mm long columns the observed failure mode was flexural, while the theory predicts failure by torsion, as shown in Fig. 9a. The discrepancy between predicted and observed failure modes at L=1400 mm is likely to be explained by reference to the magnitude of local geometric imperfection (w_{f0}). Notwithstanding that the values of w_{f0} shown in Table 6 are simply the measured mid-span values with no account given of the longitudinal variation of the local imperfection, (so that they are not directly comparable to the magnitude of local imperfection incorporated in the nonlinear local buckling analysis), they do indicate that the local imperfection varied significantly between the test specimens. To investigate the effect of local geometric imperfections, the imperfection magnitude was increased to w_{f0}=0.2 mm, resulting in the bifurcation curves shown in Fig. 9b. It can be seen that by increasing the local geometric imperfection, the critical mode becomes the flexural mode over a much wider range of lengths, indicating that the flexural tangent rigidities (EI_y, EI_{xy}) are more sensitive to local imperfections than the warping tangent rigidity (EI_ω). It can also be seen that the effect of increasing the magnitude of local imperfection is to decrease the strength for loads near and below the local buckling load, and increase the buckling strength at loads higher than the local buckling load. The increase in buckling strength is consistent with the well-known result that the stiffness of a geometrically imperfect plate element increases with the magnitude of local imperfection in the initial post-buckling range. It appears from Figs 9a and 9b that better agreement between test and numerical analysis is achieved for the 1400 mm long columns for w_{f0}=0.2 mm but the agreement is compromised at shorter lengths.

4 Conclusions

Two series of tests on thin-walled Z-section columns have been presented, one on narrow flange Z-sections and one on wide flange Z-sections. The Z-section was chosen as representative of point-symmetric cross-sections. The test specimens were uniformly compressed between fixed ends over a wide range of lengths featuring failure by interaction of local and overall flexural and/or torsional buckling. The test specimens were brake-pressed from high strength steels with nominal yield stress values of 450 MPa and 500 MPa. Coupon tests demonstrated significant material softening at stresses well below the yield stress.

The tests strengths have been compared with elastic and inelastic buckling loads predicted for locally buckled Z-sections bifurcating in an overall mode. The bifurcation loads of the narrow flange section were higher than the test strengths with increasing discrepancy in the short to intermediate length range. The discrepancy has been attributed to overall geometric imperfections present in the test specimens, gradual material softening and inability of the nonlinear finite strip analysis to model localised curvature for the number of harmonics chosen. The tests confirmed that local buckling does not produce coupling between torsion and flexure in Z-section columns.

The bifurcation loads of the wide flange specimens were generally in good agreement with the tests strengths, particularly for those columns with negligible overall geometric imperfections. The main cause of the discrepancy between the experimental and numerical strengths is attributed to gradual material softening. The experimental failure modes were also in general agreement with those predicted by the overall bifurcation analysis. In particular, the switch in overall buckling mode from the flexural to the torsional mode predicted by the bifurcation theory was confirmed by the tests. The overall bifurcation mode was shown to be sensitive to the magnitude of local imperfection. The flexural mode proved more affected by local geometric imperfections causing the flexural mode to be critical over a wide range of lengths for large local geometric imperfections compared to small local geometric imperfections.

According to the bifurcation analysis, the direction of overall buckling changes from the major principal axis in a locally buckled section. This result was verified by the narrow flange test series using a geometric nonlinear finite element analysis. However, the change in direction was less than 1° for the Z-sections tested and could not be demonstrated experimentally because of random variations in the direction of overall buckling resulting from overall geometric imperfections.

5 Acknowledgments

The narrow flange test series was conducted by Ms Anh Ton and Ms Ruth Tirtaatmadja as part of their BE honours thesis project, while the wide flange test series was conducted by Mr Robert Fish and Mr Michael Lee as part of their BE honours thesis projects. The substantial contributions from these students to this report are gratefully acknowledged.

6 References

[1] Rasmussen, KJR, Bifurcation of Locally Buckled Point Symmetric Columns - Analytical Developments, *Research Report No. R866*. 2006, School of Civil Engineering, University of Sydney: Sydney.

[2] Young, B and Rasmussen, KJR, Bifurcation of singly symmetric columns. *Thin-walled Structures*, 1997. **Vol. 28**(2): p. 155-177.

[3] Rasmussen, KJR, Bifurcation of Locally Buckled Members. *Thin-walled Structures*, 1997. **28**(2): p. 117-154.

[4] Key, PW and Hancock, GJ, A Finite Strip Method for the Elastic-Plastic Large Displacement Analysis of Thin-Walled and Cold-Formed Steel Sections. *Thin-walled Structures*, 1993. **Vol. 16**: p. 3-29.

[5] Steel Sheet and Strip—Hot–dipped Zinc–coated or Aluminium/Zinc–coated, AS1397. 1993, Standards Australia: Sydney.

[6] Hancock, GJ, Local, Distortional and Lateral Buckling of I-beams. *Journal of the Structural Division, American Society of Civil Engineers*, 1978. **Vol. 104**(ST11): p. 1787-1798.

[7] Hasham, AS and Rasmussen, KJR, Nonlinear Analysis of Locally Buckled I-section Steel Beam-columns. *Australian Journal of Structural Engineering*, 2002. **3**(3): p. 171-199.

[8] Hibbitt, Karlsson, and Sorensen, *ABAQUS Standard, Users Manual, Ver. 5.7*. Vol. Vols 1 and 2. 1997.

Tables

E_0	$\sigma_{0.01}$	$\sigma_Y=\sigma_{0.2}$	σ_u	n
(GPa)	(MPa)	(MPa)	(MPa)	
216	383	533	576	9.1

Table 1: Average tensile mechanical properties. G450 steel. Narrow flange tests.

b_f	b_w	t*	r_o	A	I_y	I_x	α	σ_l	l
(mm)	(mm)	(mm)	(mm)	(mm^2)	(mm^4)	(mm^4)		(MPa)	(mm)
26.4	121.8	1.495	3.0	256.5	9573	5.01×10^5	6.95°	137.2	120

* base metal thickness

Table 2: Average measured cross-section dimensions and section constants. Narrow flange tests.

Specimen	*Length* (L)	u_0	u_0/L	w_{w0}	N_{lE}	N_u	N_u/N_l
	(mm)	(mm)		(mm)	(kN)	(kN)	
zf250a	250	0.075	1/3330	0.28	-	65.3	1.95
zf250b	249.5	0.121	1/2060	0.00	36.0	64.5	1.83
zf600a	399.5	0.121	1/3300	0.22	35.0	61.2	1.74
zf600b	399	0.036	1/11080	0.14	38.0	61.2	1.74
zf600a	600.5	0.241	1/2490	0.15	35.5	60.2	1.71
zf600b	600	0.188	1/3190	0.14	36.0	60.1	1.71
zf800a	799	0.445	1/1800	0.25	38.0	57.3	1.63
zf800b	800.5	0.214	1/3740	0.28	36.5	57.2	1.63
zf1000a	1000	0.401	1/2500	0.30	33.0	54.5	1.55
zf1000b	1000	0.455	1/2200	0.11	34.0	51.8	1.47
zf1200a	1199	0.250	1/4800	0.30	33.5	42.5	1.21
zf1200b	1198	0.314	1/3810	0.18	32.6	44.6	1.27
zf1400a	1400.5	0.205	1/6830	0.23	-	35.5	1.01
zf1400b	1400	0.367	1/3820	0.20	-	29.5	0.838
zf1600a	1597	0.359	1/4450	0.08	-	29.0	0.824
zf1600b	1599	0.374	1/5350	0.18	-	29.8	0.847
Average			1/4050	0.19	35.3		

Table 3: Geometric imperfections and ultimate loads. Narrow flange tests.

	E_0	$\sigma_{0.01}$	$\sigma_y=\sigma_{0.2}$	σ_u	n
	(GPa)	(MPa)	(MPa)	(MPa)	
Tension	197	331	528	575	6.4
Compression	199	334	466	-	9.0

Table 4: Average mechanical properties. G450 steel. Wide flange tests

b_f	b_w	t*	r_o	A	I_y	I_x	I_ω	J	α	σ_l	l
(mm)	(mm)	(mm)	(mm)	(mm^2)	(mm^4)	(mm^4)	(mm^6)	(mm^4)		(MPa)	(mm)
42.7	44.7	1.50	2.6	190.1	1.42×10^4	1.28×10^5	1.75×10^7	141	43°	212	95

* base metal thickness

Table 5: Average measured cross-section dimensions and section constants. Wide flange tests.

Specimen	Length	u_0/L	ϕ_0	w_{f0}	N_{lE}	N_u	N_u/N_l
	(mm)		(deg)	(mm)	(kN)	(kN)	
ztf120a	119.0	-	-	-	-	64.2	1.60
ztf120b	119.0	-	-	-	43.3	55.8	1.39
ztf200a	201.0	1/46500	0.12	0.05	39.2	62.2	1.55
ztf200b	199.6	1/42800	0.13	0.01	39.8	60.9	1.51
ztf400a	400.0	1/8500	0.20	0.17	42.3	59.1	1.47
ztf400b	399.0	1/6700	0.27	0.30	39.1	58.6	1.46
ztf600a	599.0	1/115000	0.49	0.09	41.5	54.5	1.36
ztf600b	599.0	1/248000	0.71	0.69	40.8	54.6	1.36
ztf800a	799.0	1/25000	0.98	0.11	40.9	50.2	1.25
ztf800b	798.0	1/21000	0.72	0.22	44.5	50.5	1.26
ztf1000a	999.0	1/34000	0.54	0.12	41.3	46.7	1.16
ztf1000b	999.0	1/22500	0.37	0.39	41.8	44.7	1.11
ztf1200a	1199.0	1/6700	0.07	0.36	40.0	41.6	1.03
ztf1200b	1199.0	1/14000	0.61	0.23	40.0	42.3	1.05
ztf1400a	1399.0	1/11700	0.19	0.49	-	41.9	1.04
ztf1400b	1399.0	1/5000	0.57	0.05	-	38.1	0.95
ztf1600a	1600.0	1/8400	0.64	0.08	-	33.7	0.84
ztf1600b	1599.0	1/1294000	0.03	0.19	-	36.5	0.91
Average	-	1/14400	-	0.20	41.1	-	-

Table 6: Geometric imperfections and ultimate loads. Wide flange tests.

Figures

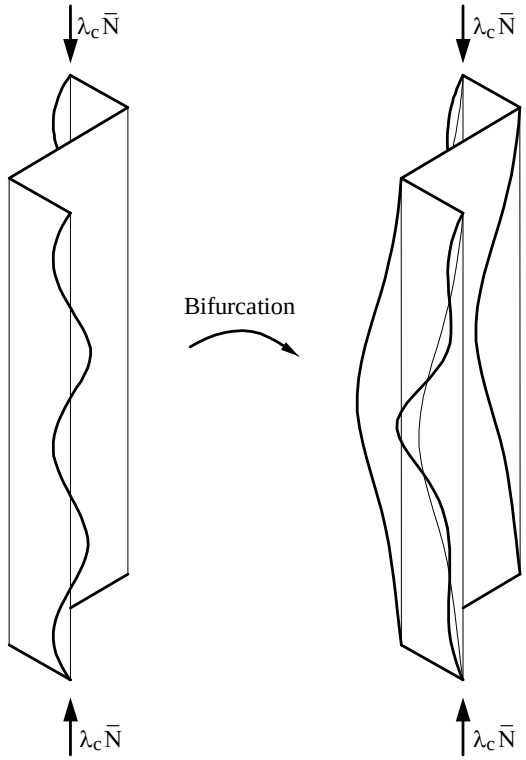

Fig. 1: Overall flexural buckling of locally buckled Z-section

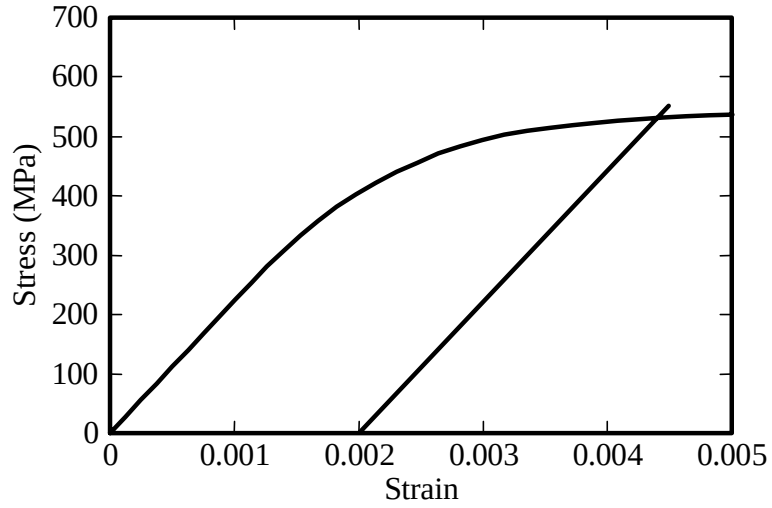

a) initial curve

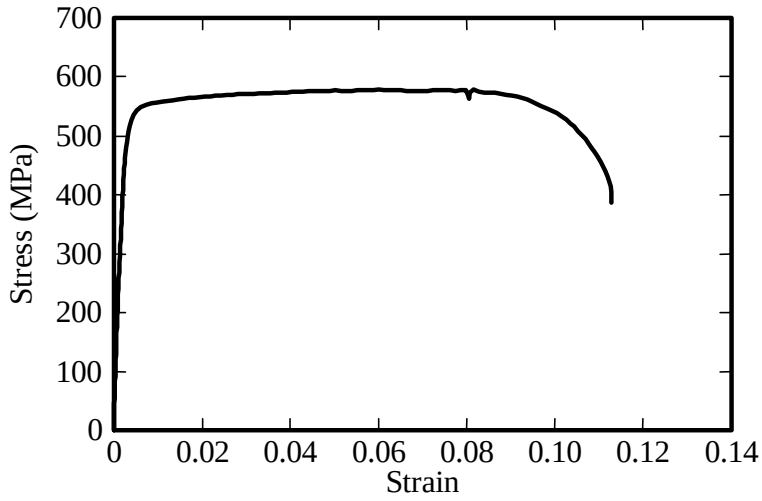

b) complete curve

Fig. 2: Typical stress-strain curve

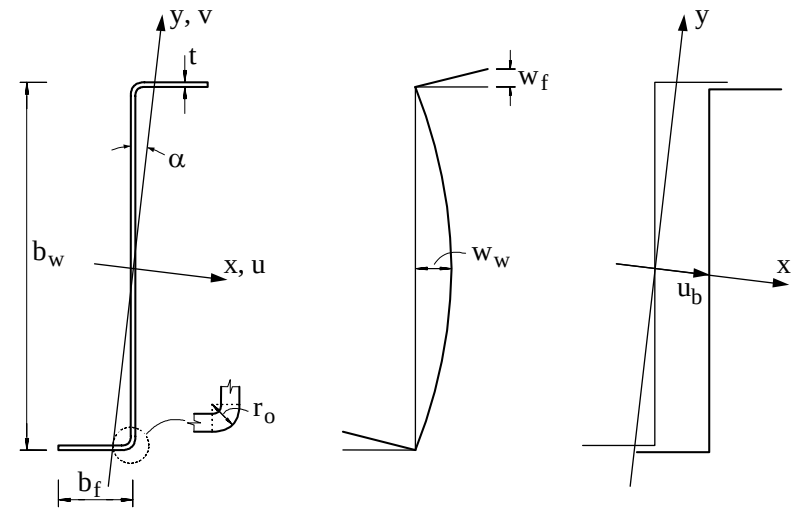

(a) Section geometry (b) Local buckling mode (c) Overall buckling mode

Fig. 3: Symbol definitions and buckling modes. Narrow flange tests.

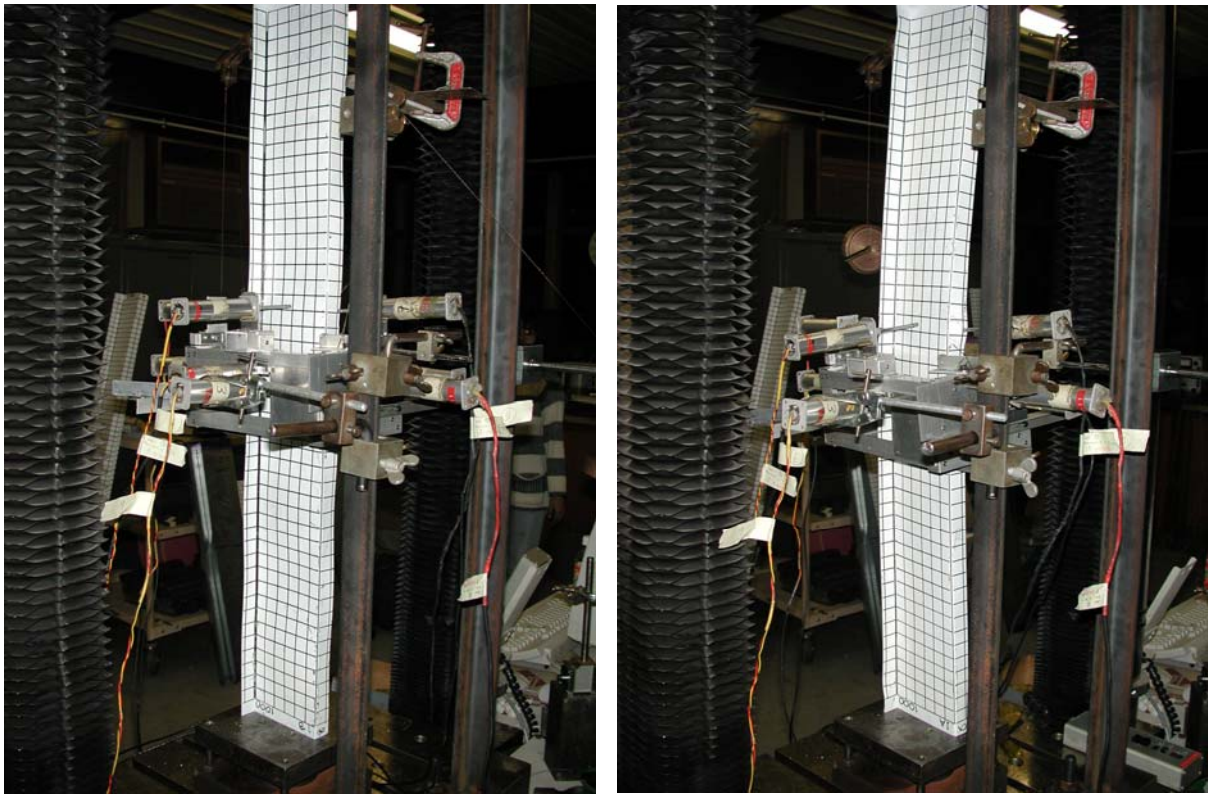

Fig. 4: Flexural buckling of locally buckled specimen zf1000a

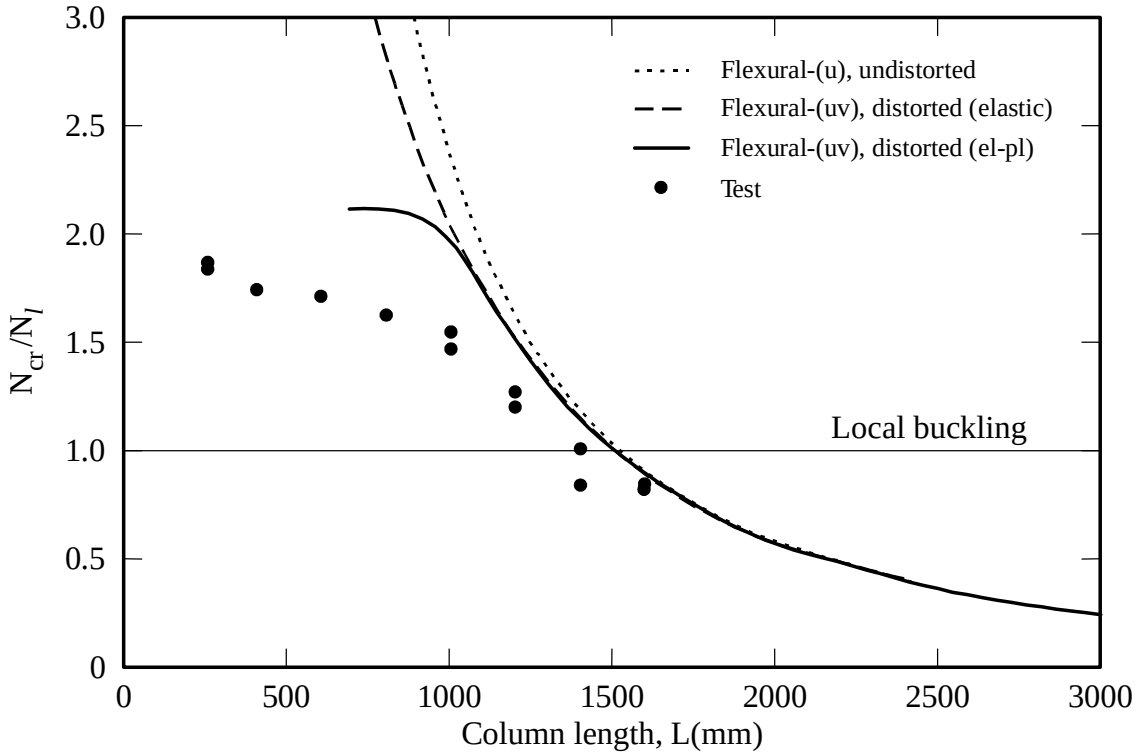

Fig. 5: Test Strengths and Bifurcation Curves. Narrow flange tests.

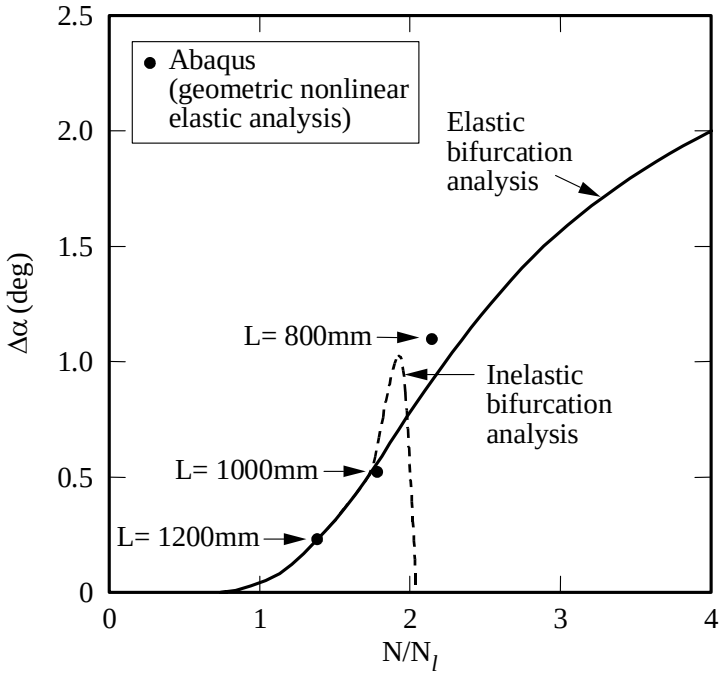

Fig. 6: Change in direction of overall buckling ($\Delta\alpha$), (positive counter-clockwise)

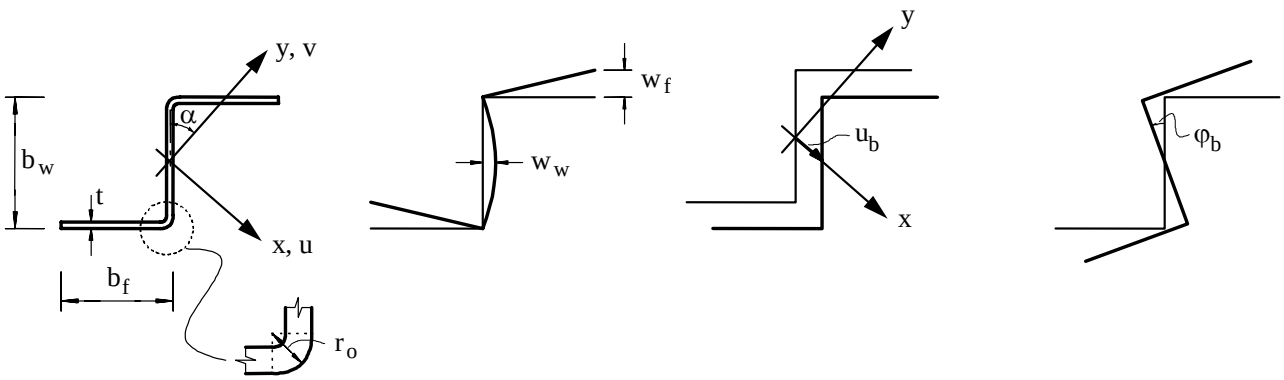

(a) Section geometry (b) Local buckling mode (c) Critical flexural buckling mode (d) Overall torsional buckling mode

Fig. 7: Symbol definitions and buckling modes. Wide flange tests

Figure 8: Specimen ztf1000b undergoing overall flexure and torsion

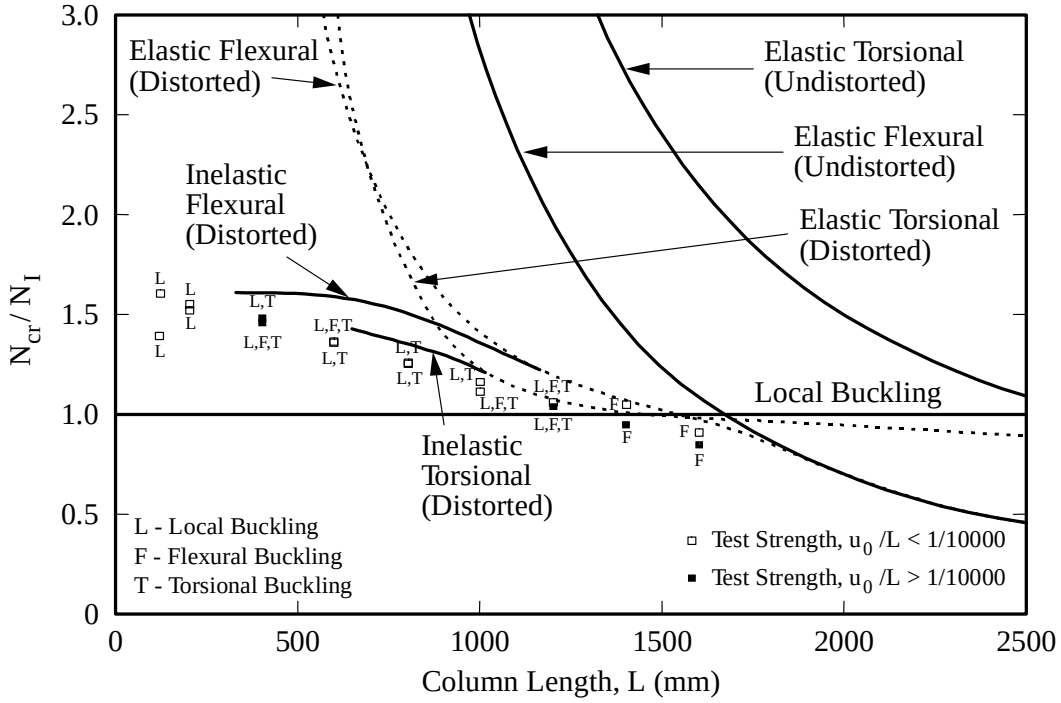

(a) Magnitude of local geometric imperfection of w_{f0}=0.02 mm in numerical analyses

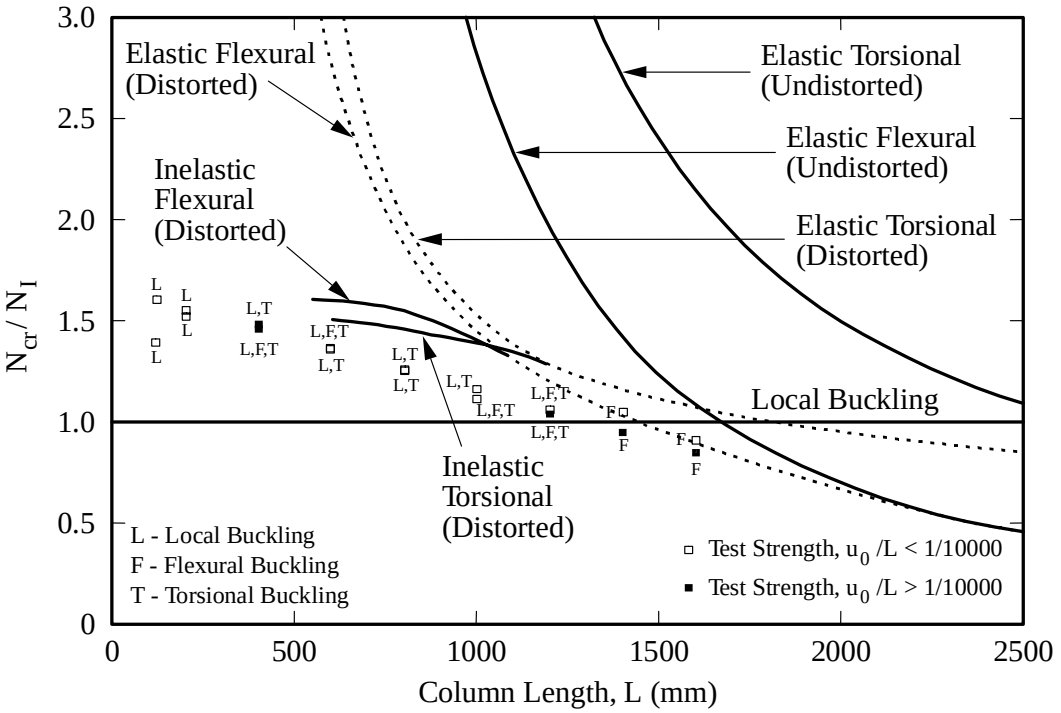

(b) Magnitude of local geometric imperfection of w_{f0}=0.2 mm in numerical analyses

Figure 9: Test strengths and bifurcation curves